IEEE Access
Multidisciplinary ⋮ Rapid Review ⋮ Open Access Journal

Received 10 June 2022, accepted 6 July 2022, date of publication 13 July 2022, date of current version 19 July 2022.

Digital Object Identifier 10.1109/ACCESS.2022.3190355

RESEARCH ARTICLE

Non-Contact Heart Rate Monitoring Based on Millimeter Wave Radar

ZONGQUAN LING[1,2], WEINAN ZHOU[1,2], YUHAO REN[1,2], JIPING WANG[2], AND LIQUAN GUO[1,2]

[1]Division of Life Sciences and Medicine, School of Biomedical Engineering (Suzhou), University of Science and Technology of China, Hefei 230026, China
[2]Suzhou Institute of Biomedical Engineering and Technology, Chinese Academy of Sciences, Suzhou 215163, China

Corresponding author: Liquan Guo (guolq@sibet.ac.cn)

This work was supported by the Key Research and Development Plan of Jiangsu Province under Grant BE2020665.

This work involved human subjects in its research. Approval of all ethical and experimental procedures and protocols was granted by the Ethics Committee of Suzhou Xiangcheng People's Hospital under Approval No. 2018 (006).

ABSTRACT Millimeter Wave(mmWave) radar has been widely used in vital sign monitoring with non-contact and privacy protection. To reduce the effect of random body motion, respiration, and its harmonics on heart rate estimation, the heart rate monitoring based on frequency-modulated continuous-wave (FMCW) radar is researched in this paper. First, a vital sign signal extraction algorithm is designed for the Range Bin variation caused by random body motion and heavy breathing. Second, a heartbeat signal extraction algorithm is designed based on Adaptive Notch Filter (ANF) and Empirical Wavelet Transform (EWT). The harmonic of respiration will be suppressed, and the heartbeat signal will be separated. Finally, the weighted estimation is performed according to the relationship of harmonics of the heartbeat signal to obtain the heart rate. Twenty subjects are invited to the experiment. The experimental results show that the proposed method can improve the signal-to-noise ratio (SNR), reduce the harmonic interference, and estimate the heart rate with a mean absolute error less than 4 BPM.

INDEX TERMS FMCW radar, heart rate estimation, ANF, EWT, the weighted estimation, the relationship of harmonics.

I. INTRODUCTION

Heart rate (HR) is an essential parameter of a human's vital signs, reflecting the physiological health state. Traditional heart rate detection devices are mainly based on electrocardiogram (ECG) or photoplethysmography (PPG). These devices must be contacted with the subject's body surface physically, which are uncomfortable to wear and have the potential for allergies [1]–[3]. In order to enhance the universality of long-term vital sign monitoring, the research on non-contact vital sign monitoring is an important topic in academia and industry [4]. The existing non-contact vital sign monitoring systems adopted optical imaging, acoustic vibration, electromagnetic waves, and other methods [5]–[7]. The electromagnetic wave-based bio-radar shows advantages in non-contact, non-invasion of privacy, and strong scalability. It has been extensively studied to search for the post-disaster survivor, monitor sleep, evaluate drivers' health in vehicles, and detect vital signs through walls [8]–[11].

Currently, there are roughly two research directions on radar-based non-contact vital sign monitoring. One is to optimize the antenna and antenna lens to suppress noise at the hardware level [4], [12]. The other is to design software-level algorithms to obtain vital sign signals with a higher signal-to-noise ratio (SNR) and more accurate frequency estimation. The radar used in non-contact vital sign monitoring is mainly composed of continuous-wave (CW) radar, impulse radio ultra-wideband (IR-UWB) radar, and frequency-modulated continuous-wave (FMCW) radar [13], [14]. FMCW Millimeter Wave (mmWave) radar has an excellent performance in distance measurement and micro-movement measurement [15], [16]. In addition, velocity measurement and angle

The associate editor coordinating the review of this manuscript and approving it for publication was Gang Wang.

measurement can be performed through the MIMO antenna arrays [17], [18]. FMCW radar detects the displacements of the chest wall caused by cardiopulmonary activity through electromagnetic waves. There are two main factors that affect the accuracy of heart rate estimation. Firstly, the heartbeat amplitude is further dampened with the buffering effect of tissues such as bones and muscles [17]. Secondly, random body motion, respiration, and harmonics affect the heartbeat signal's separation [19].

To overcome the above challenges, we propose a heart rate estimation scheme based on commodity off-the-shelf (COTS) millimeter-wave(mmWave) radar. The purpose is to suppress the interference of the random body motion, respiration, and its harmonics on the heartbeat signal at the software level and to improve the accuracy of heart rate estimation by analyzing the harmonic relationship of the heartbeat signal. The proposed signal processing algorithm consists of three parts. Firstly, a vital sign signal extraction algorithm is designed based on phase accumulation to suppress the Range Bin variation caused by random body motion and heavy breathing [15].

Adaptive Notch Filter (ANF) is combined with Empirical Wavelet Transform (EWT) to design a heartbeat signal extraction algorithm to suppress the interference of respiration and its harmonics. The respiratory harmonic components are suppressed by the ANF without affecting other features. EWT decomposes the composite signal into several band-limited sub-signals. The final heart rate estimation is then performed based on the relationship of harmonics.

The content of this paper is organized as follows: Section II reviews the related works. Section III describes the principle and feasibility of FMCW radar applied to non-contact vital signs monitoring. Section IV presents the principle of the proposed method and its performance. Section V presents the experimental results. In Section VI, we discuss the limitation and future work. This article is concluded in Section VII.

II. RELATED WORK

The two most important advantages of mmWave radar are non-contact and non-invasion of privacy, and it has excellent application prospects. This section will be divided into three aspects to introduce the related works of mmWave radar.

A. mmWAVE RADAR IMAGING

Compared with video, laser, and other methods, mmWave radar has a robust anti-jamming ability, can penetrate fog, snow, and dust, and is not affected by light [20], [21]. But the resolution of mmWave imaging is shallow, it is difficult to distinguish the target in a complex environment. Guan *et al*. proposed HawkEye, a system that leverages the cGAN architecture to recover images from low-resolution radar heatmaps [20]. To improve the accurate perception, Danzer *et al*. used PointNets to detect 2D objects based on point cloud from mmWave radar [22]. It can be used for security checks to penetrate ordinary clothing and form images of the human body and other hidden things without violating personal privacy [23].

B. APPLICATION IN MEDICINE

To adapt to global aging, the movement status and physical function of the elderly at home need to be monitored, and remote fall detection has become a popular research area [24], [25]. Jin *et al*. designed a fall detection system based on mmWave. The point cloud is used to judge abnormal spikes and centroid height drops. The detection rate is 98% in 50 fall experiments [26]. It also can be used for gait recognition and rehabilitation assessment [27]. An and Ogras proposed the mmWave-based Assistive Rehabilitation System (MARS), using CNN to reconstruct 19 human joints and bones. The mean absolute error of the joint positions is 5.87cm [28].

C. VITAL SIGN MONITORING

mmWave radar can achieve non-contact vital sign monitoring. Due to radar characteristics, the vital sign signal collected by it is susceptible to external interference. Lv *et al*. designed an antenna lens to suppress space clutter [4], [29]. It improves the accuracy of heart rate estimation, but the volume of the lens limits the integration of the antenna. Vibration FFT is applied to Range Bin selection in signal preprocessing, which is not applicable for long-term person location and increases processing time [30]. Aiming at the effect of random body motion, Tu *et al*. performed respiration monitoring based on 5.8 GHz continuous-wave (CW) radar. The subject was asked to maintain a one-dimensional(1-D) motion to generate a frequency shift. It is tough to keep a constant movement in practice, and the heart rate estimation is not performed [31]. For respiration and its harmonics, Saluja *et al*. designed a gamma filter algorithm with supervised machine learning. It was iteratively optimized based on the modified ECG signal. Its generality remains verified, and it may be necessary to increase the adaptability by increasing the filter order and samples [32]. In [18], an adaptive wavelet is designed using constellation diagrams to extract the heartbeat template, and then the continuous wavelet transform is applied to obtain the heartbeat signal. Multiple templates are required to improve the signal-to-noise ratio (SNR). EEMD has been applied to remove clutter and extract vital sign signals [33]. Still, the mode mixing is an essential factor affecting its performance, and the location of the expected signal in the IMFs is uncertain, it is necessary to screen out the vital sign signal. Time-Window-Variation Technique was applied in [11] to reduce the impact of the spectral resolution. It is needed to perform FFT multiple times, which increases time and wastes memory.

The above methods have made contributions to the signal preprocessing stage, the signal decomposition stage, and the frequency estimation stage. In this paper, the vital sign signal is extracted based on the characteristics of the time and frequency domain, which is a unique signal preprocessing. In the second stage, the ANF is combined with the EWT to obtain the heartbeat signal, which avoids the signal screening. Finally, the heartbeat spectral peak is located according to the relationship of harmonics, which can further suppress the

influence of low-frequency components on the accuracy of heart rate estimation.

III. PRINCIPLE OF FMCW RADAR

Texas Instruments (TI) IWR1843BOOST was used, which is operating across 77-81 GHz. The main structure of this system is shown in Figure 1. The signal generator produces the chirp signal, the frequency of which varies linearly with time, expressed as [34]

$$f_t = f_0 + \frac{B}{T_c}t \tag{1}$$

where f_t is the chirp frequency, f_0 is the starting frequency, B is the chirp bandwidth, and T_c is ramp time. The transmitted signal $x_T(t)$ can be obtained as

$$x_T(t) = A_T \cos\left(2\pi f_t t + \phi(t)\right) \tag{2}$$

where A_T is the transmit power and $\varphi(t)$ is the phase noise. The signal is transmitted through the TX antenna. Reflection occurs when the signal reaches the human chest wall at a distance of $d(t)$ from the antenna. The reflected signal is received, and it can be expressed as

$$x_R(t) = A_R \cos\left(2\pi f_t (t - t_d) + \phi(t - t_d)\right) \tag{3}$$

$$t_d = 2d(t)/\mathrm{c} \tag{4}$$

where $x_R(t)$ is the received signal and A_R is its amplitude. t_d represents the delay between the received signal and the transmitted signal, and c is the speed of light.

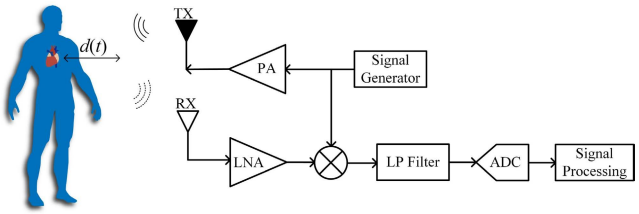

FIGURE 1. System block diagram.

The intermediate frequency (IF) signal is obtained after mixing and low-pass filtering. It can be expressed as

$$\begin{aligned} s(t) &= A\exp\left(j\left(2\pi\left(\frac{B}{T_c}t_d\right)t + 2\pi f_0 t_d \right.\right. \\ &\quad \left.\left. + \pi\frac{B}{T_c}t_d^2 + \Delta\phi(t)\right)\right) \\ &= A\exp\left(j\left(2\pi f_{IF}t + \phi_b(t) + \Delta\phi(t)\right)\right) \end{aligned} \tag{5}$$

where f_{IF} is the frequency of the IF signal

$$f_{IF} = \frac{2Bd(t)}{\mathrm{c}T_c} \tag{6}$$

and

$$\phi_b(t) = 2\pi f_0 t_d + \pi\frac{B}{T_c}t_d^2 \tag{7}$$

The residual phase noise ($\Delta\phi(t) = \phi(t) - \phi(t - t_d)$) and $\pi B t_d^2/T_c$ can be ignored in short-range applications [16], [34]. Thus, the IF signal can be rewritten as

$$s(t) = A\exp\left(j\left(2\pi\left(\frac{B}{T_c}t_d\right)t + 2\pi f_0 t_d\right)\right) \tag{8}$$

Obviously, the IF signal is sinusoidal. When the bandwidth B and the duration T_c are constant, the frequency of the IF signal only depends on the distance $d(t)$ between the antenna and the human chest wall.

For the IF signal of each chirp, N samples can be obtained by an analog-to-digital converter (ADC). The signal model is shown in Figure 2. The discrete-time sequence of the mth chirp can be written as

$$s[n, m] = A\exp\left(j\left(2\pi f_{IF} n T_f + \frac{4\pi}{\lambda}d\left(nT_f + mT_s\right)\right)\right) \tag{9}$$

where T_f corresponds to the time interval in the fast time, and T_s corresponds to the time interval in the slow time.

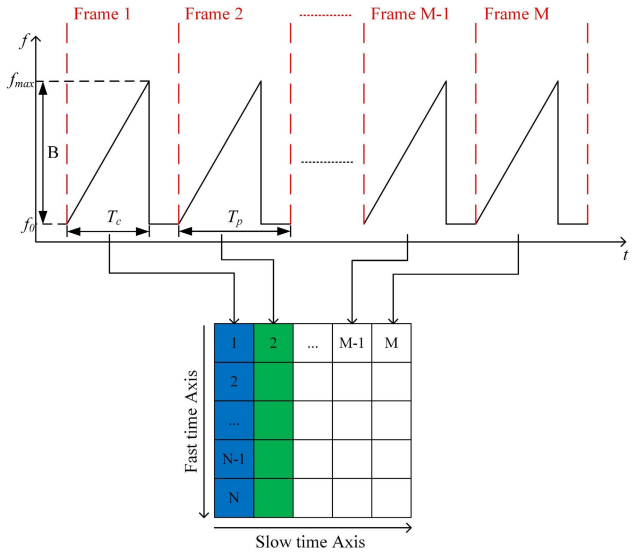

FIGURE 2. mmWave radar signal model.

The spectrum of each IF signal can be obtained by fast Fourier transform (FFT). The frequency of the spectrum represents the distance between the antenna and the subject. Its amplitude represents the intensity of the IF signal. The micro-movement of the subject is reflected in its phase. Since FFT compresses the IF signal along the distance direction, it is called Range FFT, and the unit of the spectrum is called Range Bin.

It can be seen from (6) that the frequency of the IF signal only depends on the distance between the antenna and the subject. Due to the frequency resolution of the FFT, the micro-movement of the subject cannot be obtained only by the frequency of the Range Bin. It will be reflected in the phase. The chirps are transmitted to the human body at a fixed time interval (T_p) during a period. The displacements of the chest wall caused by cardiopulmonary activity can be

obtained by extracting the phase sequence of Range Bins representing the human.

The study in this paper is based on a single person. It can be seen from the above theory that the spectrum obtained by Range FFT carries the distance and micro-movement. Single-subject vital sign monitoring can be achieved by time-frequency domain analysis.

IV. PROPOSED METHOD

Based on the above discussion, the heart rate estimation using FMCW radar generally follows the following steps:

(1) Target positioning according to the spectrum to obtain the Range Bin representing the human body.

(2) Phase extracting from the Range Bin representing the human body in each frame and Phase unwrapping to obtain vital sign signal.

(3) Decomposition of vital sign signal to obtain breathing signal and heartbeat signal.

(4) The weighted heart rate estimating based on the relationship of harmonics.

The proposed signal processing flow is shown in Figure 3. For steps (1) and (2), the Range Bin variation is caused by random body motion and heavy breathing. The vital sign signal extraction algorithm is designed to deal with it. For step (3), the heartbeat signal extraction algorithm is used. The ANF processes the vital sign signal to suppress the harmonics of respiration. The EWT decomposes it into sub-signals of different sub-passbands. Finally, for step (4), the spectral peaks are targeted in the heartbeat frequency band and the heartbeat harmonic frequency band, respectively. Their weights are updated according to the standard deviations in these two frequency bands. The heart rate is obtained by the weighted heart rate estimation.

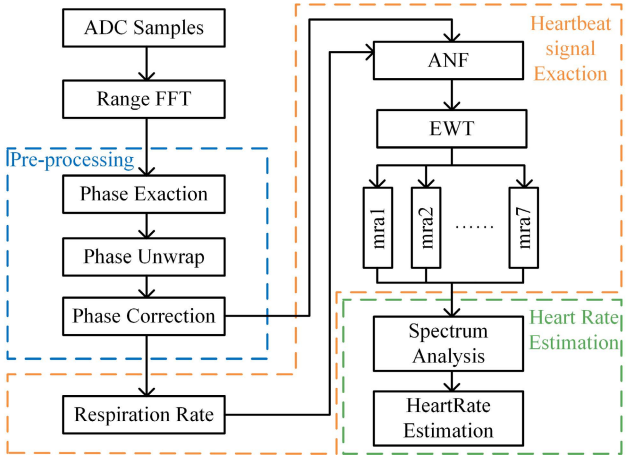

FIGURE 3. Signal processing flow.

A. VITAL SIGN SIGNAL EXTRACTION ALGORITHM

Due to the highly nonlinear phase extraction, the phase sequence data can easily contaminate [15]. The Range Bin representing the human body in each frame will not locate at the same position even if the subject does not move. The chest wall displacement caused by heavy respiration is also reflected in the spectrum. These two factors cause a step phenomenon in the unwrapped vital sign signal.

To improve the SNR, the vital sign signal extraction algorithm was designed based on phase accumulation [16]. Firstly, the Range Bin was located based on spectral energy. The principle is to calculate the sum of amplitudes of Range Bins at each distance within a time window of 3.2 seconds. The distance with the most significant sum of amplitudes was considered to represent the subject's position. The vital sign signal can be obtained by sliding the window along the slow time axis and extracting the phase of the last Range Bin in the window. Secondly, the phase is corrected based on the amplitude of chest wall displacement caused by breathing and heartbeat [36], [37]. The threshold was set empirically. If the backward differential is greater than the threshold, it is considered that the Range Bin changes at this moment. The current value will be corrected using the backward differential of the previous data.

The metal flake was driven by a stepper motor to generate the sinusoidal reciprocal motion. The Range Bin variation was simulated by adjusting the distance between the metal flake and the antenna. The experimental scenario is shown in Figure 4. The phase sequence data were extracted by a 0.05 s (only one frame in the window) time window and a 3.2 s (64 frames in the window) time window, respectively. The signals obtained with these two windows are shown in Figure 5.

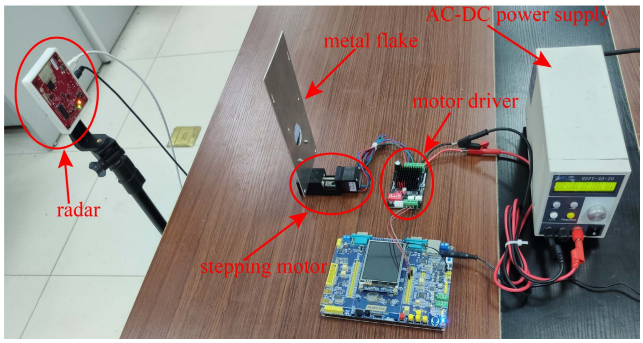

FIGURE 4. Sinusoidal reciprocal motion generated by stepper motor detected with mmWave radar.

Figure 5(a) and (b) are the time-domain waveform and spectrum of the signal obtained with the 0.05 s window, respectively. Figure 5(c) and (d) show the time-domain waveform and spectrum of the signal obtained with the 3.2 s window, respectively. It is found that the Range Bin variation causes a regular step in the phase sequence data. The SNR is calculated as follows

$$\mathrm{SNR} = 10 * \lg\left(\frac{E_{\mathrm{signal}}}{E_{\mathrm{signal}} + E_{\mathrm{noise}}}\right) \tag{10}$$

where E_{signal} is the signal energy and E_{noise} is the noise energy. The SNR of these two signals is -16 dB and -39 dB,

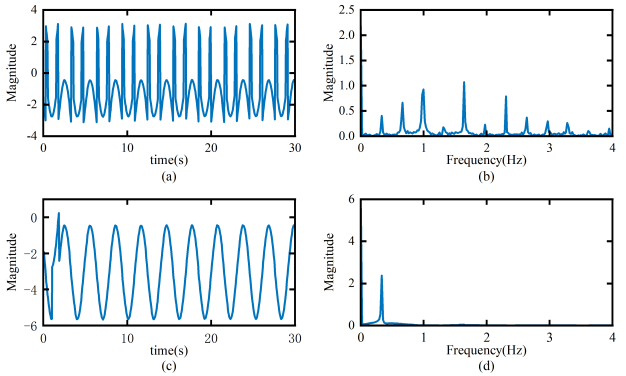

FIGURE 5. Preprocessed phase sequence data. (a) The signal obtained with the 0.05 s window. (b) The spectrum of the signal obtained with the 0.05 s window. (c) The signal obtained with the 3.2 s window. (d) The spectrum of the signal obtained with the 3.2 s window.

respectively. It is found that the proposed method can improve the SNR.

Figure 6 shows the time-frequency domain characteristics of the vital sign signal before and after phase correction. It can be seen from Figure 6(a) and Figure 6(c) that the step phenomenon in the signal is suppressed. Figure 6(c) and Figure 6(d) show that the heartbeat spectrum peak of the corrected signal is more prominent.

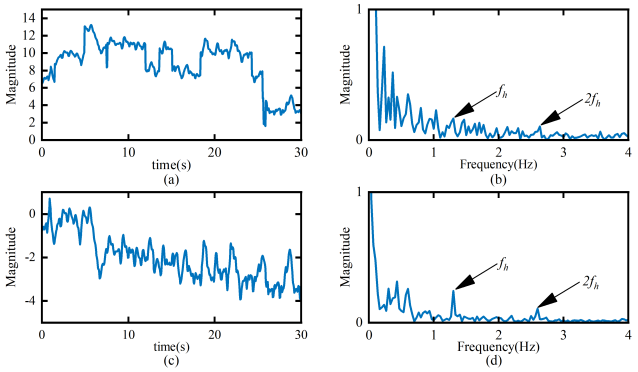

FIGURE 6. Vital sign signal before and after phase correction. (a) The time-domain waveform of uncorrected signal. (b) The spectrum of the uncorrected signal. (c) The time-domain waveform of corrected signal. (d) The spectrum of corrected signal.

B. HEARTBEAT SIGNAL EXTRACTION ALGORITHM BASED ON ANF AND EWT

The vital sign signal reflected as chest wall displacement contains respiratory and heartbeat signals and harmonics of respiration and heartbeat. At rest, the respiratory frequency of a healthy adult is [0.1-0.5] Hz, and the heartbeat frequency is [0.8-2] Hz [36]. When the respiratory rate is fast, the first harmonic of respiration may fall into the heartbeat frequency band and affect the heart rate estimation. This paper used ANF to suppress the respiratory harmonic.

The principle of ANF is to generate two mutually orthogonal reference signals under a given notch frequency. The two orthogonal signals will be accumulated with different linear combinations. The error signal $e(k)$ between the output signal $y(k)$ and the input signal $s(k)$ will be used to adjust the linear combination. The notch filter with narrow notch bandwidth and large zero-depth is achieved by subtracting the input signal $s(k)$ and the output signal $y(k)$ [29], [38]. The error signal $e(k)$ is the notched signal, and the notch frequency is ω_0. The structure of the ANF is shown in Figure 7.

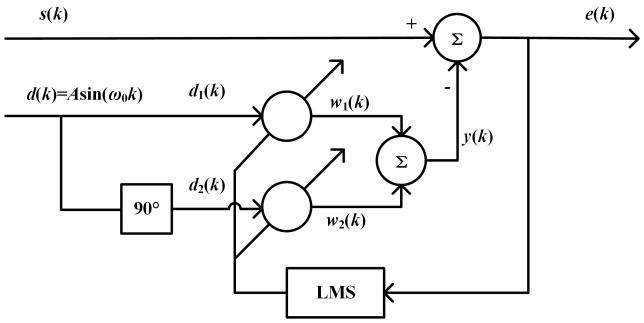

FIGURE 7. Adaptive Notch filter structure diagram.

According to the respiratory frequency band, the respiratory spectral peaks can be targeted, and then the frequency of respiratory harmonics can be obtained. Since the frequency of the second harmonic and the third harmonic is highly close to the heartbeat frequency, only the first harmonic is notched by the ANF.

Figure 8(a) is the spectrum of the vital sign signal without notch processing, and Figure 8(b) is the spectrum notched by the ANF. f_b is the respiratory frequency, $2f_b$ is the first respire tory harmonic frequency. f_h is the heartbeat frequency, and $2f_h$ is the first heartbeat harmonic frequency. Obviously, the first respiratory harmonic is suppressed and the other components are almost unaffected.

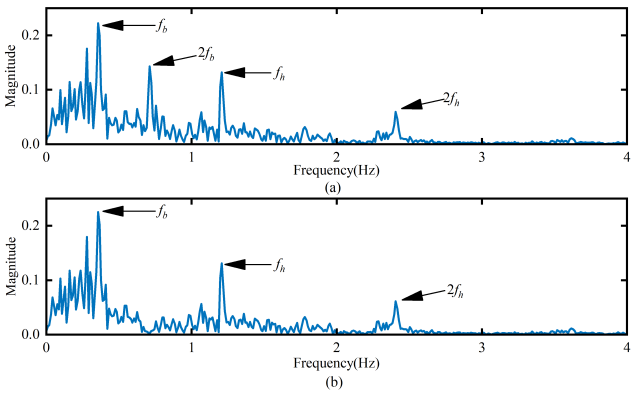

FIGURE 8. Spectrum of the vital sign signal before and after the ANF. (a) Before the notch processing. (b) After the notch processing.

EWT is a new method of constructing adaptive wavelets proposed by Gilles in 2013. Its main idea is to achieve bandpass filtering of multiple sub-passbands by constructing wavelet filter banks and extract different components

in the signal [39]. EWT has shown excellent performance in decomposing non-stationary signals, which effectively remove noise and extract interesting signal components. It has been used in image processing, disease diagnosis, and other fields [40]–[42].

The specific method that EWT achieves adaptive decomposition of the signal is to segmenting the spectrum into multiple sub-passbands based on the local maxima and local minima. It is assumed that the expected number of segments is N_0, since the two boundaries of 0 and π have been determined, the remaining N_0-1 boundaries need to be located. If the number of local maxima in the spectrum is M, the final segment number N is

$$N = \min(M + 1, N_0) \tag{11}$$

The number of decomposed sub-signals cannot exceed the number of modes contained in the input signal. The boundaries of each segment can be defined according to the selected continuous local maxima and local minima, and finally, N sub-passbands can be obtained.

Based on the above segmentation strategy, a set of empirical wavelets on the N sub-passbands can be constructed as $\{\phi_1(t), \psi_n(t)_{n=1}^N\}$, where $\phi_1(t)$ is the scaling function and $\psi_n(t)_{n=1}^N$ are the empirical wavelets.

The signal is decomposed according to the wavelet transform theory, and the signal's detail coefficients and approximation coefficients can be obtained, respectively. The detail coefficients are

$$D(n,t) = \langle s, \psi_n \rangle = \int s(\tau)\,\psi_n^*(\tau - t)\,d\tau \tag{12}$$

The approximation coefficients are

$$A(0,t) = \langle s, \phi_1 \rangle = \int s(\tau)\,\phi_1^*(\tau - t)\,d\tau \tag{13}$$

where * represents conjugation. The sub-signals can be reconstructed as

$$s_n(t) = D(n,t) * \psi_n(t) \tag{14}$$
$$s_0(t) = A(0,t) * \phi_1(t) \tag{15}$$

Spectrum segmentation is shown in Figure 9. The vital sign signal after notch processing is decomposed by EWT. The initial boundaries of EWT are set to 0.1 Hz, 0.5 Hz, 0.8 Hz, 2 Hz, 1.6 Hz, and 4 Hz. The final boundaries are redefined by locating the local minima of the spectrum around these six boundaries. The heartbeat signal will appear in the 4th EWT component, and the first heartbeat harmonic will appear in the 6th EWT component.

Figure 10 shows the respiration signal decomposed by EWT with a frequency of 0.36 Hz. Figure 11 shows the heartbeat signal and its first harmonic. It can be seen from the spectrum that the heartbeat frequency is 1.2 Hz, and the first harmonic frequency is 2.4 Hz. Figure 12 shows the heartbeat signal obtained by the radar and the ECG signal obtained by the ECG sensor synchronously. It can be seen that these two signals are strongly correlated.

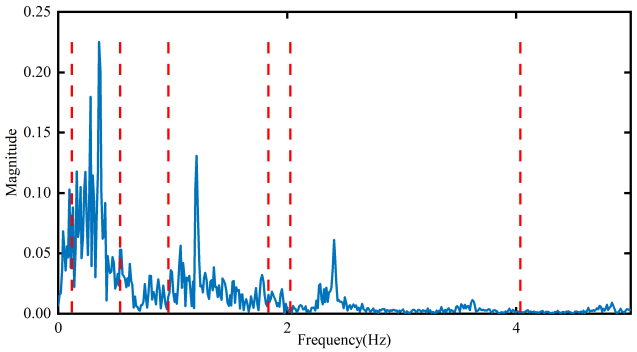

FIGURE 9. Spectrum segmentation.

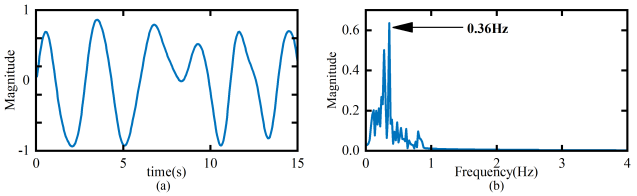

FIGURE 10. Respiratory signal. (a) Time-domain (b) Frequency-domain.

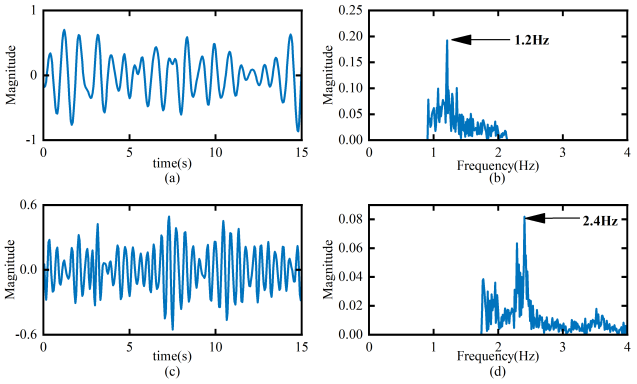

FIGURE 11. Heartbeat signal and its first harmonic. (a) Heartbeat signal. (b) The spectrum of heartbeat signal. (c) The first heartbeat harmonic. (d) The spectrum of the first heartbeat harmonic.

C. WEIGHTED HEART RATE ESTIMATION BASED ON THE RELATIONSHIP OF HARMONICS

The heartbeat signal extraction algorithm based on ANF and EWT can improve the SNR of the heartbeat signal. However, due to the small heartbeat amplitude and the wide frequency band, the heartbeat signal is easy to be contaminated by random body motion, respiration, and its harmonics. Estimating the heart rate by locating the highest spectral peak in the heartbeat frequency band is not always correct. The second and third harmonics of respiration are usually negligible [43]. It is feasible to improve the accuracy of the heart rate estimation combined with the heartbeat harmonic. Therefore, the weighted estimation based on the harmonic relationship of the heartbeat signal is proposed.

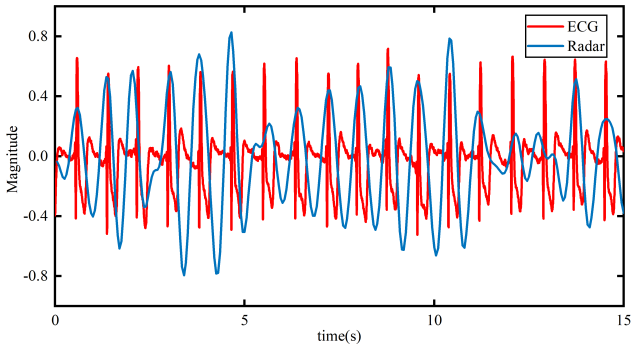

FIGURE 12. Comparison of heartbeat signal time-domain waveforms extracted by ECG and Radar.

First, the amplitude and index of each potential spectral peak of heartbeat are stored in the matrix M_1

$$M_1 = \begin{bmatrix} p_{1,1}, p_{1,2}, \cdots, p_{1,n} \\ l_{1,1}, l_{1,2}, \cdots, l_{1,n} \end{bmatrix} \tag{16}$$

where $p_{1,n}$ is the amplitude of the nth spectral peak in the heartbeat band, and $l_{1,n}$ is its index. The amplitude and index of each potential spectral peak of the first heartbeat harmonic can be obtained in the same way.

$$M_2 = \begin{bmatrix} p_{2,1}, p_{2,2}, \cdots, p_{2,m} \\ l_{2,1}, l_{2,2}, \cdots, l_{2,m} \end{bmatrix} \tag{17}$$

where $p_{2,m}$ is the amplitude of the mth spectral peak in the first heartbeat harmonic band and $l_{2,m}$ is its index.

Based on the SNR of the spectral peaks in M_1 and M_2, the spectral peaks in these two frequency bands are weighted. The standard deviations of the first four highest spectral peaks in M_1 and M_2 are calculated after sorting M_1 and M_2 in descending order of amplitude. The SNR is reflected in the standard deviation. M_1 and M_2 are weighted based on the ratio of these two standard deviations.

$$M_1' = \eta_1 M_1 \tag{18}$$

$$M_2' = \begin{bmatrix} \eta_2 & 0 \\ 0 & 1/2 \end{bmatrix} M_2 \tag{19}$$

$$\begin{cases} \eta_1 = \dfrac{\text{std}_1}{\text{std}_1 + \text{std}_2} \\ \eta_2 = \dfrac{\text{std}_2}{\text{std}_1 + \text{std}_2} \end{cases} \tag{20}$$

where std_1 and std_2 are the standard deviations of the spectral peaks in the two frequency bands.

The weighted accumulation matrix M can be obtained by adding the amplitudes of the spectral peaks whose index difference between M_1' and M_2' is less than 0.1 Hz (corresponding to a heart rate of 6 BPM) [44].

The index of the spectral peak representing the heartbeat in the weighted accumulation matrix M is

$$\text{index} = \arg\max_i (\boldsymbol{P}) \tag{21}$$

The heartbeat frequency can be obtained as

$$f_h = \frac{(L[\text{index}] - 1) f_s}{N} \tag{22}$$

where f_h is the heartbeat frequency, f_s is the sampling frequency, and N is the number of data in the window.

As the random body motion and the interference of breathing, there are usually multiple spectral peaks in the heartbeat frequency band. The heartbeat spectral peaks in Figure.13(a) and Figure.13(c) are weaker than the low-frequency components, and the harmonic weighted accumulation targets the correct spectral peaks.

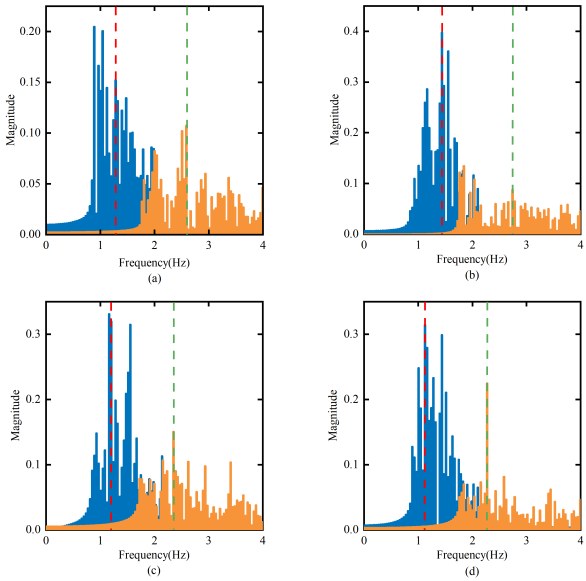

FIGURE 13. Four examples of heartbeat spectral peak location. (a), (c) Heartbeat spectral peaks are weaker than other components. (b), (d) Heartbeat spectral peaks are stronger than other components. The red line is the heartbeat spectral peak, and the green line is the first harmonic spectral peak.

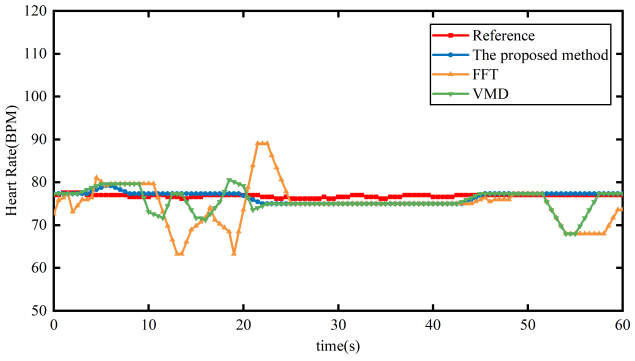

FIGURE 14. Heart rate comparison curve.

Figure 14 shows the heart rate estimation obtained by three different methods and the reference heart rate from the ECG sensor. Figure 15 shows the absolute error distribution of these three methods. The proposed method can track the heart rate variation with an accuracy of 98% and a uniform error distribution, which is better than the other two methods. The

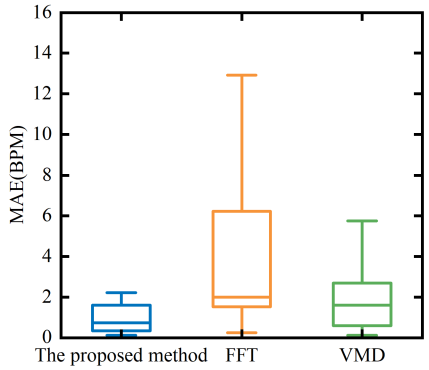

FIGURE 15. Absolute error of heart rate estimation for different methods.

FFT-based method and the VMD-based method are interfered by noises such as respiration harmonics and random body motion.

V. EXPERIMENTS AND RESULTS

A. EXPERIMENTAL SETUP

The IWR1843BOOST is used for data acquisition, which is equipped with four receive antennas and three transmit antennas, and the parameters are set as shown in Table 1. The radar used in this paper has a small antenna size and refined Range Bin [15], [45]. The amplitude of the chest wall caused by the heartbeat is 0.1-0.5 mm, and the back amplitude is 0.01-0.2 mm [37]. Combined with phase analysis, heartbeat detection can be achieved.

TABLE 1. Radar parameters.

Parameter	Value
Start Frequency	77GHz
Slope	76MHz/μs
ADC Sampling time	50μs
Band Width	3.8GHz
ADC Samples	256
ADC Sampling Rate	5120KSPS
Frame Frequency	20Hz
Range Resolution	0.04m
Chirp Numbers	4

The experiment is carried out indoors. The experimental equipment includes Texas Instruments (TI) IWR1843BOOST, a computer (CPU i7-7700@3.6 GHz 16 GB RAM) equipped with MATLAB R2021a, and a contact ECG sensor (NeuroSky BMD101). ECG signal is acquired synchronously using an ECG sensor at the subject's chest. The experiment duration is about 90 s, the time window is 25.6 s, and the step is 0.5 s. Twenty subjects are invited to participate in the experiment, as shown in Figure 16(b).

The proposed method is a traditional signal processing method, the collected data are used to test the accuracy of the method.

The mean absolute error (MAE) and the mean absolute percentage error (MAPE) are used to evaluate the accuracy

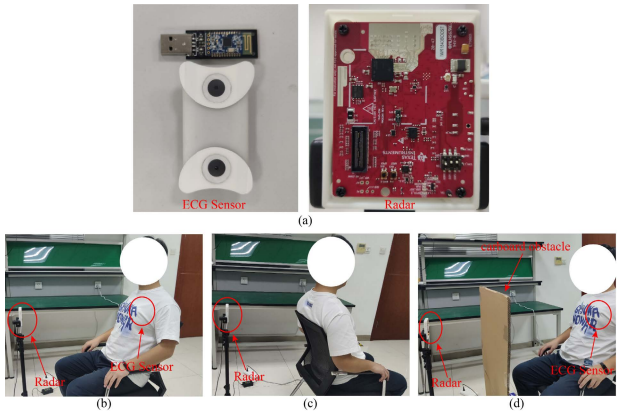

FIGURE 16. Experimental scenarios. (a) Devices. (b)Front. (c) Back. (d) With obstacle.

of heart rate estimation. The calculation formula of MAE is

$$\mathrm{MAE} = \frac{\sum_{i=1}^{N} abs\left(\mathrm{HR_{ECG}}\left(i\right) - \mathrm{HR_{radar}}\left(i\right)\right)}{N} \tag{23}$$

The formula for calculating MAPE is

$$\mathrm{MAPE} = \frac{\sum_{i=1}^{N} \left(\frac{abs(\mathrm{HR_{ECG}}(i) - \mathrm{HR_{radar}}(i))}{\mathrm{HR_{ECG}}(i)}\right)}{N} \times 100\% \tag{24}$$

B. OVERALL PERFORMANCE

Table 2 lists the heart rate estimation of 20 subjects sitting and facing to radar, including the average heart rate, MAE and MAPE. Compared with the contact sensor, the MAE for heart rate estimation is less than 4 BPM, and the MAPE is less than 5%.

C. THE EFFECTS OF OTHER FACTORS ON ACCURACY

In this section, the effects of distance, orientation, and obstacle on the accuracy are investigated. As shown in Figure 17(a) and Figure 17(b), the subjects face the radar and turn their backs to the radar, respectively, and sit in 4 positions within 0.5-2 m from the radar for testing. The MAE and MAPE are listed in Table 3. Figure 17(c) gives the MAE distribution of different orientations and distances. The heart rate estimation accuracy of the mmWave radar can reach 98% within the range of 2 m. Within this range, the attenuation of electromagnetic waves does not have a significant impact on the accuracy.

As shown in Figure 18 (a), the cardboard was placed between the antenna and the subject, and the distance between the subject and the antenna was changed. MAE distribution is given in Figure 18(b). The MAE and MAPE are listed in Table 4. The cardboard obstacle causes the attenuation of the signal, but the influence on the accuracy of heart rate estimation is not evident within the range of 2 m.

A comparison of radar systems and methods used in non-contact vital sign monitoring studies by various research

TABLE 2. Estimation results using the proposed method.

Subject	Age	BMI	ECG AVE.HR(BPM)	Radar AVE.HR(BPM)	MAE(BPM)	MAPE(%)
1	25	29.0	73	72	0.802	1.110
2	24	24.2	77	76	0.809	1.049
3	26	24.6	77	75	1.070	1.360
4	24	22.3	80	79	0.998	1.254
5	25	21.2	63	62	0.940	1.518
6	24	25.7	103	103	0.964	0.932
7	24	31.5	88	88	1.013	1.162
8	25	22.2	69	69	0.895	1.287
9	25	22.9	63	63	3.076	4.902
10	22	26.1	68	67	1.235	1.812
11	27	22.5	73	73	0.688	0.952
12	31	18.7	86	86	0.784	0.910
13	20	22.4	76	75	0.788	1.039
14	24	24.8	72	70	3.056	4.260
15	34	20.3	88	87	1.059	1.204
16	26	22.6	76	74	2.365	3.099
17	24	21.6	62	62	0.964	1.556
18	26	20.4	83	82	1.481	1.796
19	28	22.0	77	76	0.920	1.199
20	25	22.5	75	74	1.708	2.305
Average					1.281	1.735

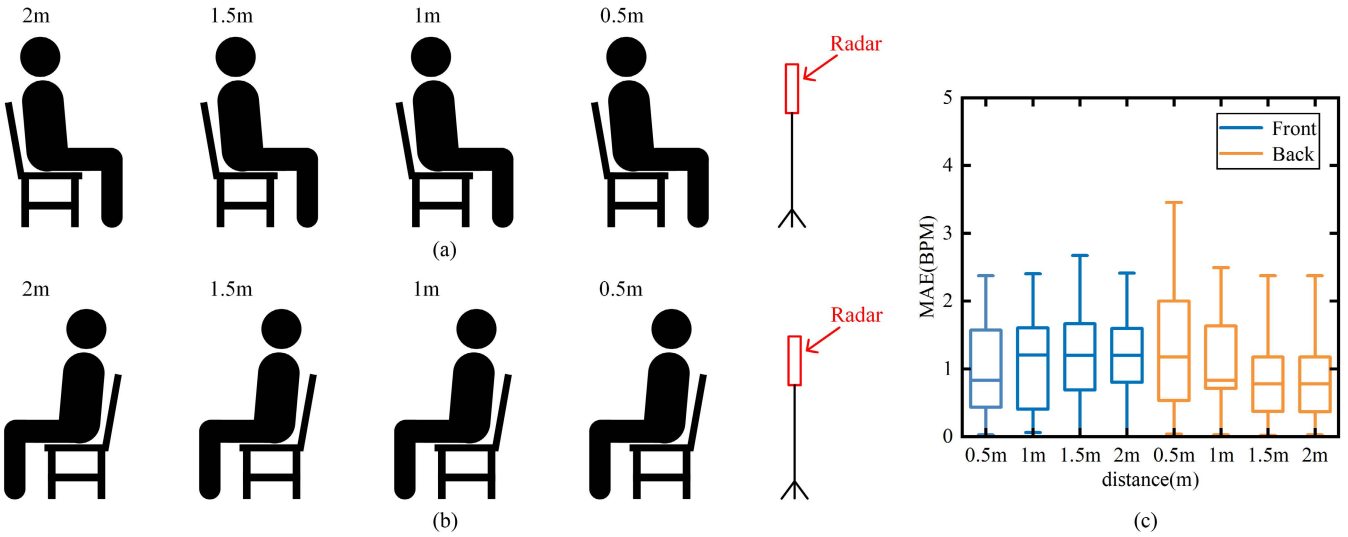

FIGURE 17. Experimental setup and MAE distribution. (a) Front. (b) Back. (c) MAE distribution of different orientations and distances.

TABLE 3. Heart rate estimation results in different orientations and distances.

Orientation	Distance(m)	MAE(BPM)	MAPE(%)
Front	0.5	0.986	1.46
	1	1.049	1.750
	1.5	1.316	1.792
	2	1.183	1.587
Back	0.5	1.347	1.925
	1	1.130	1.624
	1.5	0.889	1.353
	2	0.841	1.254

TABLE 4. Heart rate estimation results in the presence of the obstacle.

Distance	MAE(BPM)	MAPE(%)
1m	0.861	1.355
1.5m	1.621	2.138
2m	1.655	2.155

groups is summarized in Table 5. The proposed method can achieve satisfactory results. Compared with [4], the time required for both works is approximate, but our method suppresses noise during signal preprocessing and avoid the model training. It reduces the hardware cost and size associated with the antenna lens and impact of other parameters. Lv *et al.* [29] achieves comparable accuracy to our method, but our method avoids the signal screening. Both [30] and ours use a 77GHz FMCW radar, but our heart rate estimation time is much shorter than [30], and the accuracy is higher. Saluja *et al.* [32] used machine learning methods to optimize

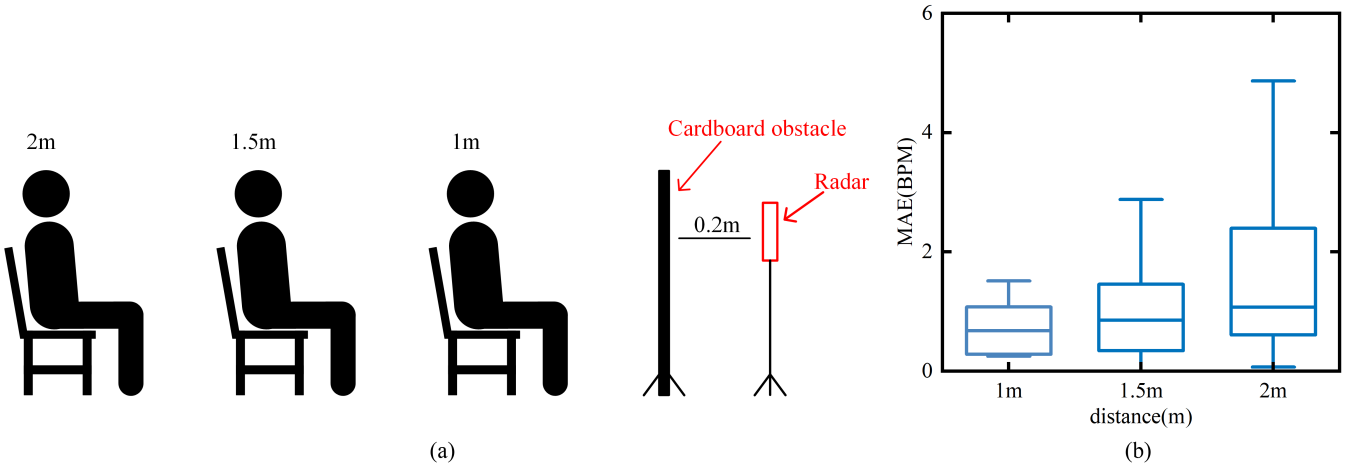

FIGURE 18. Experimental setup and MAE distribution. (a) Experimental scenario. (b) MAE distribution of different distances with the obstacle.

TABLE 5. Comparison of the heart rate estimation results with other works.

Ref.	Radar	D.(m)	T.(s)	Method	ACC.(%)
[4]	120GHz FMCW	1	3	SR	95.62
[29]	120GHz FMCW	1	3	CEEMD AN	97
[30]	77GHz FMCW	1.7	12.8	FFT	80
[32]	5.8GHz CW	0.1-3	<1	Gamma Filter	96.4
[46]	N/A	1.5	N/A	PD	92.5
ours	77GHz FMCW	0.5-2	2.8	our method	98

D., detection distance; T., reported estimation time; ACC., reported average accuracy of heart rate.

filter, and although it achieved a comparable accuracy, our method does not need model training and is more universal. In [46], they also research the effect of distance and orientation on the accuracy, but the estimation of our method is more accurate.

VI. LIMITATIONS AND FUTURE WORK

This paper researches the non-contact heart rate monitoring based on 77GHz FMCW radar. The results show that the proposed method has satisfactory performance and is conducive to the application of non-contact vital sign monitoring. The method proposed in this paper has some shortcomings. Firstly, the current work is single-person vital sign monitoring. Secondly, the heartbeat signal is not filtered more finely, there is still noise, and there may be a significant effect in the heart rate variability analysis. Finally, the effect of ground truth device attached to the human chest wall on radar sensing has not been studied intensely.

The above limitations will be investigated in the future. Firstly, the multi-subject vital signs monitoring will be researched. Secondly, the heartbeat signal extraction algorithm will be optimized to improve the SNR. Finally, the robustness of experimental scenarios will be studied to enhance the universality of mmWave radar.

VII. CONCLUSION

A heart rate estimation scheme based on 77GHz FMCW radar was designed. A vital sign signal extraction algorithm was proposed, and the reliability was proved. The ANF was used to suppress the first respiratory harmonic, and then the signal was decomposed by EWT. Finally, the weights were changed based on the harmonic relationship and then estimated the heart rate. The experimental result of 20 subjects showed that the MAE of the heart rate estimated by the proposed method is less than 4 BPM. The effects of orientation, distance, and obstacle on the accuracy were studied, which shows that the proposed method can obtain accurate results in different scenarios. It demonstrated that the proposed method improves the accuracy of FMCW radar in non-contact vital sign monitoring.

REFERENCES

[1] M. Kebe, R. Gadhafi, B. Mohammad, M. Sanduleanu, H. Saleh, and M. Al-Qutayri, "Human vital signs detection methods and potential using radars: A review," *Sensors*, vol. 20, no. 5, p. 1454, Mar. 2020.
[2] W. Zhang, G. Li, Z. Wang, and H. Wu, "Non-contact monitoring of human heartbeat signals using mm-wave frequency-modulated continuous-wave radar under low signal-to-noise ratio conditions," *IET Radar, Sonar Navigat.*, vol. 16, no. 3, pp. 456–469, Mar. 2022.
[3] P. Zhao, C. X. Lu, B. Wang, C. Chen, L. Xie, M. Wang, N. Trigoni, and A. Markham, "Heart rate sensing with a robot mounted mmWave radar," in *Proc. IEEE Int. Conf. Robot. Autom. (ICRA)*, May 2020, pp. 2812–2818.
[4] W. Lv, Y. Zhao, W. Zhang, W. Liu, A. Hu, and J. Miao, "Remote measurement of short-term heart rate with narrow beam millimeter wave radar," *IEEE Access*, vol. 9, pp. 165049–165058, 2021.
[5] X. Yang, B. Yang, Z. Wang, Y. Zhang, H. Zhou, X. Li, and S. Cao, "Progress in clinical application of non-contact vital signs monitoring technology," *Med. Inf.*, vol. 31, no. 18, pp. 41–44, Sep. 2018.
[6] Y. Jing, Y. Cao, M. Zhu, T. Lei, J. Xia, Z. Li, L. Zhang, J. Wang, and G. Lu, "Research status and development of non-contact life detection technology," *China Med. Devices*, vol. 36, no. 6, pp. 1–4, 2021.
[7] P. Hou, N. Li, and T. Song, "Research status and development of life detection technology," *Transducer Microsyst. Technol.*, vol. 33, no. 7, pp. 1–8, 2014.

[8] J. Li, L. Liu, Z. Zeng, and F. Liu, "Advanced signal processing for vital sign extraction with applications in UWB radar detection of trapped victims in complex environments," *IEEE J. Sel. Topics Appl. Earth Observ. Remote Sens.*, vol. 7, no. 3, pp. 783–791, Mar. 2014.

[9] Z. Li, T. Jin, Y. Dai, and Y. Song, "Through-wall multi-subject localization and vital signs monitoring using UWB MIMO imaging radar," *Remote Sens.*, vol. 13, no. 15, p. 2905, Jul. 2021.

[10] Z. Yang, P. H. Pathak, Y. Zeng, X. Liran, and P. Mohapatra, "Vital sign and sleep monitoring using millimeter wave," *ACM Trans. Sensor Netw.*, vol. 13, no. 2, pp. 1–32, May 2017.

[11] J. Tu and J. Lin, "Fast acquisition of heart rate in noncontact vital sign radar measurement using time-window-variation technique," *IEEE Trans. Instrum. Meas.*, vol. 65, no. 1, pp. 112–122, Jan. 2016.

[12] G. Sacco, E. Piuzzi, E. Pittella, and S. Pisa, "An FMCW radar for localization and vital signs measurement for different chest orientations," *Sensors*, vol. 20, no. 12, p. 3489, Jun. 2020.

[13] M. Nosrati, S. Shahsavari, S. Lee, H. Wang, and N. Tavassolian, "A concurrent dual-beam phased-array Doppler radar using MIMO beamforming techniques for short-range vital-signs monitoring," *IEEE Trans. Antennas Propag.*, vol. 67, no. 4, pp. 2390–2404, Apr. 2019.

[14] I. Nejadgholi, H. Sadreazami, S. Rajan, and M. Bolic, "Classification of Doppler radar reflections as preprocessing for breathing rate monitoring," *IET Signal Process.*, vol. 13, no. 1, pp. 21–28, Feb. 2019.

[15] L. Sun, S. Huang, Y. Li, C. Gu, H. Pan, H. Hong, and X. Zhu, "Remote measurement of human vital signs based on joint-range adaptive EEMD," *IEEE Access*, vol. 8, pp. 68514–68524, 2020.

[16] Y. Hu and T. Toda, "Remote heart-rate estimation based on phase accumulation-linear interpolation method for mm-wave FMCW radar," *IEICE Commun. Exp.*, vol. 10, no. 2, pp. 56–61, Feb. 2021.

[17] F. Wang, X. Zeng, C. Wu, B. Wang, and K. J. R. Liu, "mmHRV: Contactless heart rate variability monitoring using millimeter-wave radio," *IEEE Internet Things J.*, vol. 8, no. 22, pp. 16623–16636, Nov. 2021.

[18] T. K. V. Dai, Y. Yu, P. Theilmann, A. E. Fathy, and O. Kilic, "Remote vital sign monitoring with reduced random body swaying motion using heartbeat template and wavelet transform based on constellation diagrams," *IEEE J. Electromagn., RF Microw. Med. Biol.*, vol. 8, no. 22, pp. 1–8, Jan. 2022.

[19] M. Mabrouk, S. Rajan, M. Bolic, M. Forouzanfar, H. R. Dajani, and I. Batkin, "Human breathing rate estimation from radar returns using harmonically related filters," *J. Sensors*, vol. 2016, pp. 1–7, Jan. 2016.

[20] J. Guan, S. Madani, S. Jog, S. Gupta, and H. Hassanieh, "Through fog high-resolution imaging using millimeter wave radar," in *Proc. IEEE/CVF Conf. Comput. Vis. Pattern Recognit. (CVPR)*, Jun. 2020, pp. 11464–11473.

[21] R. Appleby, D. A. Robertson, and D. Wikner, "Millimeter wave imaging: A historical review," *Proc. SPIE*, vol. 10189, May 2017, Art. no. 1018902.

[22] A. Danzer, T. Griebel, M. Bach, and K. Dietmayer, "2D car detection in radar data with PointNets," in *Proc. IEEE Intell. Transp. Syst. Conf. (ITSC)*, Oct. 2019, pp. 61–66.

[23] Z. Wang, T. Chang, and H.-L. Cui, "Review of active millimeter wave imaging techniques for personnel security screening," *IEEE Access*, vol. 7, pp. 148336–148350, 2019.

[24] R. Z. Morawski, A. Miękina, and P. R. Bajurko, "Measurement data preprocessing in a radar-based system for monitoring of human movements," *J. Phys., Conf. Ser.*, vol. 588, pp. 1–9, Feb. 2015.

[25] M. Mercuri, P. J. Soh, G. Pandey, P. Karsmakers, G. A. Vandenbosch, P. Leroux, and D. Schreurs, "Analysis of an indoor biomedical radar-based system for health monitoring," *IEEE Trans. Microw. Theory Techn.*, vol. 61, no. 5, pp. 2061–2068, May 2013.

[26] F. Jin, A. Sengupta, and S. Cao, "mmFall: Fall detection using 4-D mmWave radar and a hybrid variational RNN autoencoder," *IEEE Trans. Autom. Sci. Eng.*, vol. 19, no. 2, pp. 1245–1257, Apr. 2022.

[27] M. Z. Ozturk, C. Wu, B. Wang, and K. J. R. Liu, "GaitCube: Deep data cube learning for human recognition with millimeter-wave radio," *IEEE Internet Things J.*, vol. 9, no. 1, pp. 546–557, Jan. 2022.

[28] S. An and U. Y. Ogras, "MARS: mmWave-based assistive rehabilitation system for smart healthcare," *ACM Trans. Embedded Comput. Syst.*, vol. 20, no. 5s, pp. 1–22, Oct. 2021.

[29] W. Lv, W. He, X. Lin, and J. Miao, "Non-contact monitoring of human vital signs using FMCW millimeter wave radar in the 120 GHz band," *Sensors*, vol. 21, no. 8, p. 2732, Apr. 2021.

[30] M. Alizadeh, G. Shaker, J. C. M. De Almeida, P. P. Morita, and S. Safavi-Naeini, "Remote monitoring of human vital signs using mm-wave FMCW radar," *IEEE Access*, vol. 7, pp. 54958–54968, 2019.

[31] J. Tu, T. Hwang, and J. Lin, "Respiration rate measurement under 1-D body motion using single continuous-wave Doppler radar vital sign detection system," *IEEE Trans. Microw. Theory Techn.*, vol. 64, no. 6, pp. 1937–1946, Jun. 2016.

[32] J. Saluja, J. Casanova, and J. Lin, "A supervised machine learning algorithm for heart-rate detection using Doppler motion-sensing radar," *IEEE J. Electromagn., RF Microw. Med. Biol.*, vol. 4, no. 1, pp. 45–51, Mar. 2020.

[33] K.-K. Shyu, L.-J. Chiu, P.-L. Lee, T.-H. Tung, and S.-H. Yang, "Detection of breathing and heart rates in UWB radar sensor data using FVPIEF-based two-layer EEMD," *IEEE Sensors J.*, vol. 19, no. 2, pp. 774–784, Jan. 2019.

[34] M. Mercuri, I. R. Lorato, Y.-H. Liu, F. Wieringa, C. Van Hoof, and T. Torfs, "Vital-sign monitoring and spatial tracking of multiple people using a contactless radar-based sensor," *Nature Electron.*, vol. 2, pp. 252–262, Jun. 2019.

[35] A. Ahmad, J. C. Roh, D. Wang, and A. Dubey, "Vital signs monitoring of multiple people using a FMCW millimeter-wave sensor," in *Proc. IEEE Radar Conf.*, Apr. 2018, pp. 1450–1455.

[36] A. De Groote, M. Wantier, G. Cheron, M. Estenne, and M. Paiva, "Chest wall motion during tidal breathing," *J. Appl. Physiol.*, vol. 83, no. 5, pp. 1531–1537, Nov. 1997.

[37] K. Liu, C. Ding, and Y. Zhang, "A coarse-to-fine robust estimation of FMCW radar signal for vital sign detection," in *Proc. IEEE Radar Conf.*, Sep. 2020, pp. 1–6.

[38] S. Ishibashi, S. Koshita, M. Abe, and M. Kawamata, "DSP implementation of adaptive notch filters with overflow avoidance in fixed-point arithmetic," in *Proc. Asia–Pacific Signal Inf. Process. Assoc. Annu. Summit Conf. (APSIPA ASC)*, Nov. 2018, pp. 1355–1360.

[39] J. Gilles, "Empirical wavelet transform," *IEEE Trans. Signal Process.*, vol. 61, no. 16, pp. 3999–4010, Aug. 2013.

[40] X. Zhang, X. Yang, Y. Ding, Y. Wang, J. Zhou, and L. Zhang, "Contactless simultaneous breathing and heart rate detections in physical activity using IR-UWB radars," *Sensors*, vol. 21, no. 16, p. 5503, Aug. 2021.

[41] W. Liu and W. Chen, "Recent advancements in empirical wavelet transform and its applications," *IEEE Access*, vol. 7, pp. 103770–103780, 2019.

[42] M. He, Y. Nian, L. Xu, L. Qiao, and W. Wang, "Adaptive separation of respiratory and heartbeat signals among multiple people based on empirical wavelet transform using UWB radar," *Sensors*, vol. 20, no. 17, p. 4913, Aug. 2020.

[43] M. Le and B. Van Nguyen, "Multivariate correlation of higher harmonics for heart rate remote measurement using UWB impulse radar," *IEEE Sensors J.*, vol. 20, no. 4, pp. 1859–1866, Feb. 2020.

[44] H. Xu, M. P. Ebrahim, K. Hasan, F. Heydari, P. Howley, and M. R. Yuce, "Accurate heart rate and respiration rate detection based on a higher-order harmonics peak selection method using radar non-contact sensors," *Sensors*, vol. 22, no. 1, p. 83, Dec. 2021.

[45] D. M. Pozar and F. Croq, "Millimeter-wave design of wide-band aperture-coupled stacked microstrip antennas," *IEEE Trans. Antennas Propag.*, vol. 39, no. 12, pp. 1770–1776, Dec. 1991.

[46] Y. Xiong, S. Chen, X. Dong, Z. Peng, and W. Zhang, "Accurate measurement in Doppler radar vital sign detection based on parameterized demodulation," *IEEE Trans. Microw. Theory Techn.*, vol. 65, no. 11, pp. 4483–4492, Nov. 2017.

ZONGQUAN LING received the B.E. degree in biomedical engineering from Chongqing University, Chongqing, China, in 2020. He is currently pursuing the M.Sc. degree with the University of Science and Technology of China. His research interests include vital signs algorithm and embedded systems.

WEINAN ZHOU received the B.E. degree in biomedical engineering from Army Medical University, Chongqing, China, in 2022. He is currently pursuing the M.Sc. degree with the University of Science and Technology of China. His research interest includes intelligent rehabilitation assessment.

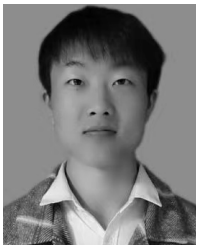

YUHAO REN received the B.E. degree in applied physics from Xi'an Jiaotong University, Xi'an, China, in 2020. He is currently pursuing the M.Sc. degree with the University of Science and Technology of China. His research interest includes intelligent rehabilitation assessment.

JIPING WANG received the B.E. degree in applied physics and the M.S. degree in condensed matter physics from Xi'an Jiaotong University, Xi'an, China, in 2008 and 2011, respectively. His current research interests include intelligent rehabilitation and assisted assessment.

LIQUAN GUO received the master's degree from the Graduate School, Chinese Academy of Sciences, in 2010. He is currently pursuing the Ph.D. degree with the University of Science and Technology of China. He is a Professor and the Master Tutor with the University of Science and Technology of China. His research interests include medical electronics and intelligent rehabilitation engineering.